Polyoxymethylene-Homopolymer/Hydroxyapatite Nanocomposites for Biomedical Applications

Kinga Pielichowska

Faculty of Materials Science and Ceramics, Department of Biomaterials, AGH University of Science and Technology, Al. Mickiewicza 30, 30-059 Kraków, Poland

Received 8 September 2010; accepted 24 April 2011
DOI 10.1002/app.34752
Published online 23 August 2011 in Wiley Online Library (wileyonlinelibrary.com).

ABSTRACT: In this article, new polyoxymethylene (POM)/hydroxyapatite (HAp) nanocomposites for bone long-term implants have been obtained and characterized by using FTIR, WAXD, SEM, TG, DSC, tensile tests, and *in vitro* evaluation. Characteristic bands both for extended chain crystals (ECC) and folded chain crystals (FCC) were observed in FTIR profiles for both pure POM and POM in POM/HAp nanocomposites. From WAXD analysis it has been found that the addition of HAp does not change the hexagonal system of POM in POM/HAp nanocomposites. Moreover, degree of crystallinity of POM increases with an increase of HAp content up to 1.0% and next decreases with an increase HAp content. It indicates that HAp nanoparticles up to 1.0% content act as effective nucleating sites. Mechanical tests revealed that Young's modulus increases, whereby, elongation at break and tensile strength decrease with increasing hydroxyapatite concentration. Results of *in vitro* investigations show that an increase of HAp content in POM nanocomposites facilitates formation of apatite layer on the sample surface and improves *in vitro* stability POM/HAp nanocomposites. © 2011 Wiley Periodicals, Inc. J Appl Polym Sci 123: 2234–2243, 2012

Key words: biomaterials; nanocomposites; thermal properties; crystallization; mechanical properties

INTRODUCTION

Bone exhibits a complex structural hierarchy that spans over nanometer to millimeter. At the nanostructural level, bone is primarily composed of hydroxyapatite (HAp) and collagen. HAp mineralizes at specific locations at collagen, in such a way that the c-axis of HAp aligns parallel to collagen molecule. The collagen molecule is helical overall with non-helical ends that are N- or C-telopeptides.[1] A variety of materials have been used for replacement and repair of damaged or traumatized bone tissues—metals, ceramics, and polymers.[2,3] In the latter group, the scaffolds for bone tissue engineering should be fabricated from a biocompatible polymer, which does not have the potential to elicit an immunological or foreign body reaction. The chosen polymer can degrade at a controlled rate in concert with tissue regeneration. The degradation products should not be toxic and must be easily excreted by metabolic pathways.[4]

Nanocomposites consisting of a polymer matrix and HAp provide specific biomaterials for internal bone implants with biological and mechanical properties tailored for a given medical use. These materials link the advantages of polymers (structural stability, strength, biocompatibility, desired shape) with properties of HAp that resembles bone structure.[5,6]

Polyoxymethylene (POM) belongs to the group of engineering thermoplastics; it is also called polyacetal because of its basic molecular structure consisting of a repeating carbon-oxygen linkage. Acetal homopolymer refers to resin containing solely the carbon-oxygen backbone, while for the copolymer resin the oxymethylene structure is occasionally interrupted by a comonomer unit.[7] Properties which arise from polyacetal structure are: high-impact strength, stiffness, resiliency, toughness, and high yield stress; low friction coefficient; low gas and vapour permeability; exceptional dimensional stability and dielectric properties; high fatigue strength; and good retention of properties at elevated temperature.[8] POM shows an ultra high modulus—it is caused by the presence of extended-chain crystals, whereby a part of the polymer could still appear as chain-folded lamellae.[9]

Recently, some novel POM-based (nano)composites have been described in the literature. Hence, Sanchez-Soto et al.[10] investigated the influence of the functionalization of fully condensed polyhedral oligomeric silsesquioxanes (POSS) on the properties of

Correspondence to: K. Pielichowska (kingapie@agh.edu.pl).

Contract grant sponsor: Polish Ministry of Science and Higher Education; contract grant number: PBZ/MEiN/01/2006/15.

POM-based nanocomposites and they found that the thermal stability under inert atmosphere of POM dramatically increased with the addition of POSS moieties. Masirek and Piórkowska[11] studied nucleation of crystallization process of polyoxymethylene with dispersed submicron particles of poly(tetrafluoroethylene) (PTFE). POM with PTFE particles are all-polymer systems with enhanced nucleation of crystallization; PTFE particles with sizes below 300 nm added to POM efficiently decreased sizes of polycrystalline aggregates. In another development, Siengchin et al.[12] obtained binary and ternary composites composed of POM, polyurethane (PU), and carbon nanofibers (CNF) by water-mediated melt compounding. Authors revealed that CNF worked as reinforcement and also improved the thermo-oxidative stability of POM. POM/multiwalled carbon nanotube (MWNT) nanocomposites prepared through a solution-evaporation method assisted by ultrasonic irradiation showed improved thermal conductivity.[13]

Polyacetal has been used in different joints, but also as heart valve replacements. While it is a well-known engineering polymer and has been applied previously in orthopaedic implants (in e.g., hip and knee prostheses), there is little data on the effect of long-term exposure to the physiological environment on its mechanical properties.[14,15] Moore et al.,[16] suggested the possibility of using polyacetal instead of metal for the femoral component of knee prosthesis. Polyacetal homopolymer has also been used as the occluder disc of the Björk-Shiley Delrin® (BSD) heart valve.[17] Moreover, POM has been used for more than two decades in dentistry as a substitute for acrylic resins and metals in many prosthetic applications. Cytotoxicity studies and intracutaneous reactivity studies of pedodontic POM crowns were performed at NAMSA (Northwood, OH), and the results showed, under the conditions of these studies, no evidence of cytotoxicity or allergenic reactions.[18]

In this work it is reported on novel POM/hydroxyapatite nanocomposites for bone long-term implants that have been obtained using melt processing technique.

EXPERIMENTAL

Materials and processing

A commercial grade of POM homopolymer (Delrin®), with melt flow rate (MFR 190/2.16, ISO 1133) of 2.4 g/10 min, was supplied by Du Pont. Hydroxyapatite $Ca_{10}(PO_4)_6OH_2$ nanopowder with a nanoparticle size below 100 nm (99% of particles) was product of nGimat (Atlanta, USA).

POM and POM/HAp nanocomposites were prepared by melt processing method. First, POM was air-dried, and then the POM and HAp were mechanically mixed (0, 0.5, 1.0, 2.5, 5, and 10.0% w/w of HAp) and extruded in a double screw extruder (Thermo-Haake PolyLab PTW 16/25) at a rotary speed of 50 rpm. The temperature profiles of the barrel were 212–220–220–215°C. Compositions were then shaped by using DSM laboratory injection moulding machine.

Techniques

Microstructure and spectroscopic characterization

Scanning electron microscope (SEM) Phillips XL 30, equipped with an energy dispersive X-ray analyser (Link ISIS-EDX) was used to investigate the surface morphology of carbon-coated samples at the energy of the electron beam of 5 kV. WAXD measurements were performed using Philips X'Pert Pro MD diffractometer. Radiation used was Cu Kα1 line monochomatized by Ge(111) monochromator. Standard Bragg–Brentano geometry with Θ-2Θ setup was applied (0.008° step size and 15°–60° 2HΘ range). All measurements were performed at room temperature. IR spectra of the samples were recorded at elevated temperatures using a HATR PIKE attachment with ZnSe crystal on a Bio-Rad FTS 165 Fourier transform infrared (FTIR) spectrometer at a resolution of 2 cm^{-1}.

Thermal properties

For the DSC measurements Mettler-Toledo DSC 822e, operating in dynamic mode, was employed. The conditions were: samples of about 5 mg, the heating/cooling rate of 10 K min^{-1}, atmosphere: argon, intracooler was used for cooling. As a lower temperature limit the point of first deflection on the DSC curve from the baseline level was assumed, while as upper temperature limit the point where the (heat flow) profile comes back to baseline was taken (the first derivative curve is used to confirm the temperature range, too). To calculate the heat of melting of polymer matrix, the normalized enthalpy of melting of nanocomposites was divided by weight fraction of POM in nanocomposite. Thermogravimetric analysis was performed on a Netzsch TG 209 thermal analyzer, operating in a dynamic mode at a heating rate of 10 K min^{-1}. The conditions were: sample weight, about 5 mg; atmosphere, argon; open a-Al_2O_3 pan.

Tensile testing

Mechanical tests were carried out using a Zwick machine in the tensile mode at upper crosshead speed of 50 mm min^{-1} at ambient temperature according to PN-EN ISO 527. Tensile specimens according to PN-EN ISO 3167 with thickness 1.53 ± 0.02 mm and width 4.91 ± 0.01 mm were applied.

Young's modulus of the samples was determined from the slope of the stress-strain function at its linear part. The yield strength was determined from the upper yield point and the fracture strain was the elongation at break from the tensile curve. The reported mechanical properties were calculated by averaging measurements of three specimens.

In vitro evaluation

POM an POM/HAp nanocomposite specimens were immersed in a simulated body fluid (SBF) at 37°C for 3 and 7 days. After soaking, the specimens were removed from the SBF, gently rinsed with distilled water and dried.[19] After SBF immersion, the sample surface was examined by SEM-EDX.

Moreover, POM and POM/10,0% HAp samples were incubated at the temperature of 70°C according to EN ISO 10993-13 during 41 weeks in the Ringer fluid, made by Baxter Terpol (biological environment simulation) and distilled water. The pH, conductivity and the mass change were measured during incubation.

RESULTS AND DISCUSSIONS

Structure and morphology

POM has a hexagonal unit cell with unit cell dimensions of $a = b = 4.45$ Å and $c = 17.3$ Å.[20] The molecular chains are arranged in a 9/5 helix where a and b axes are on the same plane and the chains are aligned parallel to the c axis of the crystal.[21] For POM, the calculated positions of the peaks in the 2θ scan are 22.9°, 34.6°, 48.4°, and 54.1° for diffraction planes having Miller indices (100), (105), (115), and (205), respectively.[22,23] The X-ray diffraction patterns for POM and POM/HAp nanocomposites are shown in Figure 1.

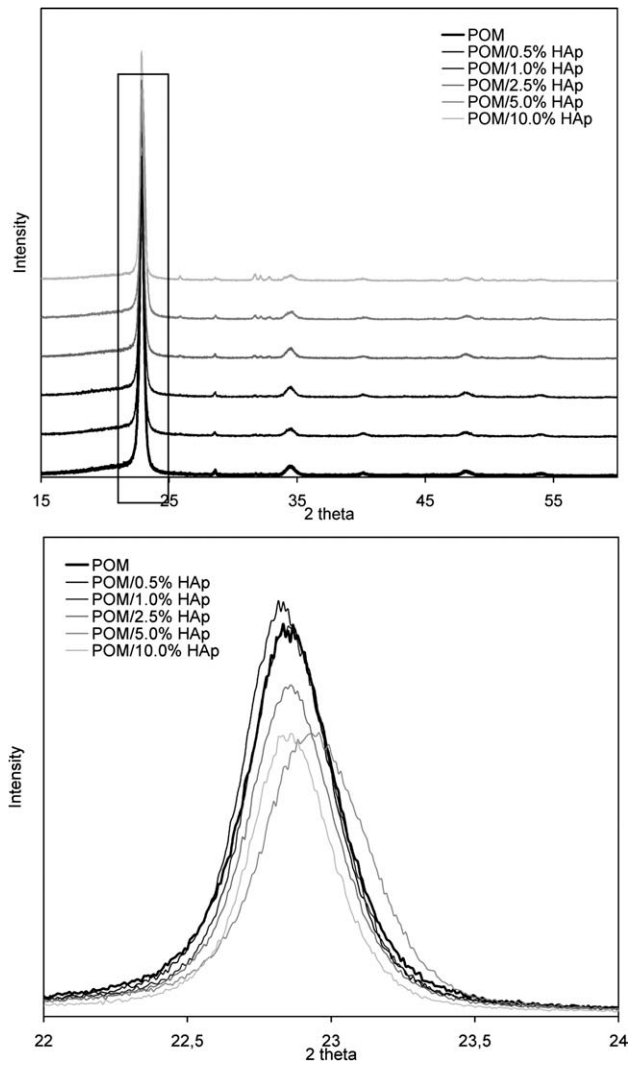

Figure 1 WAXD diffraction patterns of POM and POM/HAp nanocomposites.

No shift in 2θ for pure POM and POM with hydroxyapatite was observed, indicating that the addition of HAp does not change the hexagonal system of POM.[24] Figure 7(b) shows the 2Θ vs. scattering intensity plots from the (100) plane for POM and POM/HAp nanocomposites after injection moulding. The intensity of the reflections from the (100) plane changes with the HAp content in samples because of the change in the degree of crystallinity.[25,26] The highest intensity was observed for POM/0.5% HAp, lower intensities were observed for POM and POM/1% HAp, and for other samples with an increase of HAp content intensity of the peak decreased—it stay in good agreement with DSC results.

Another point to be discussed is a complex morphology of POM and its nanocomposites, with extended chain crystal (ECC) and folded chain crystal (FCC) structures. FCC of POM was found in the dilute solutions at an early stage of discovery of polymer single crystals,[24,27,28] whereby ECC of POM was found as a product of cationic polymerization of trioxane.[29] Shish-kebab structure or a hybrid structure of ECC and FCC was also observed for the oriented overgrowth crystallization of the molten POM on the needle-shaped POM single crystal.[30] The morphology of POM depends very much on the sample preparation conditions. The infrared spectra of POM are known to be highly sensitive to the morphology of the crystallites, and for example, Shimomura and Iguchi[31–33] discovered a remarkable difference in the infrared spectra between ECC and FCC. POM samples prepared by cooling the melt exhibits the ECC bands more clearly, allowing to speculate that the POM sample crystallized from the melt is a mixture of ECC and FCC in a complicated manner. In the cooling process from the melt, Hama and Tashiro found that the infrared bands characteristic

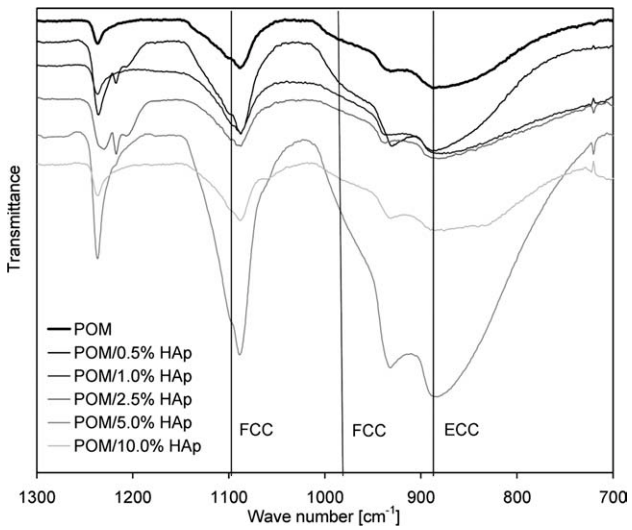

Figure 2 FTIR-ATR spectra of POM and POM/HAp nanocomposites.

of folded chain crystal (FCC) morphology appeared around 156°C, followed by a gradual increase of infrared bands of extended chain crystal (ECC) around 140°C.[34,35] Moreover, they found that the lamellar stacking structure formed during primary crystallization becomes tighter during secondary crystallization by a generation of second lamellae in between the original lamellae—so-called lamellar insertion model was adopted here as the most possible structure model of POM sample crystallized from the melt. Moreover, they speculated, the fully extended chains may be produced by applying tensile or shear stress along the chain axis during the crystallization process.[36] Figure 2 shows infrared spectra taken for the POM and POM/HAp nanocomposites.

Characteristic bands both for ECC and FCC were observed in spectral profiles of POM and POM/HAp nanocomposites, but no significant differences in shape of spectral profiles between pure POM and POM/HAp nanocomposites. It means that in nanocomposite samples POM also crystallize as FCC and ECC. The fracture surfaces of POM and POM/HAp nanocomposites are presented in Figure 3.

It is believed that voids appear to be concentrated within this spherulitic structure, leading to the

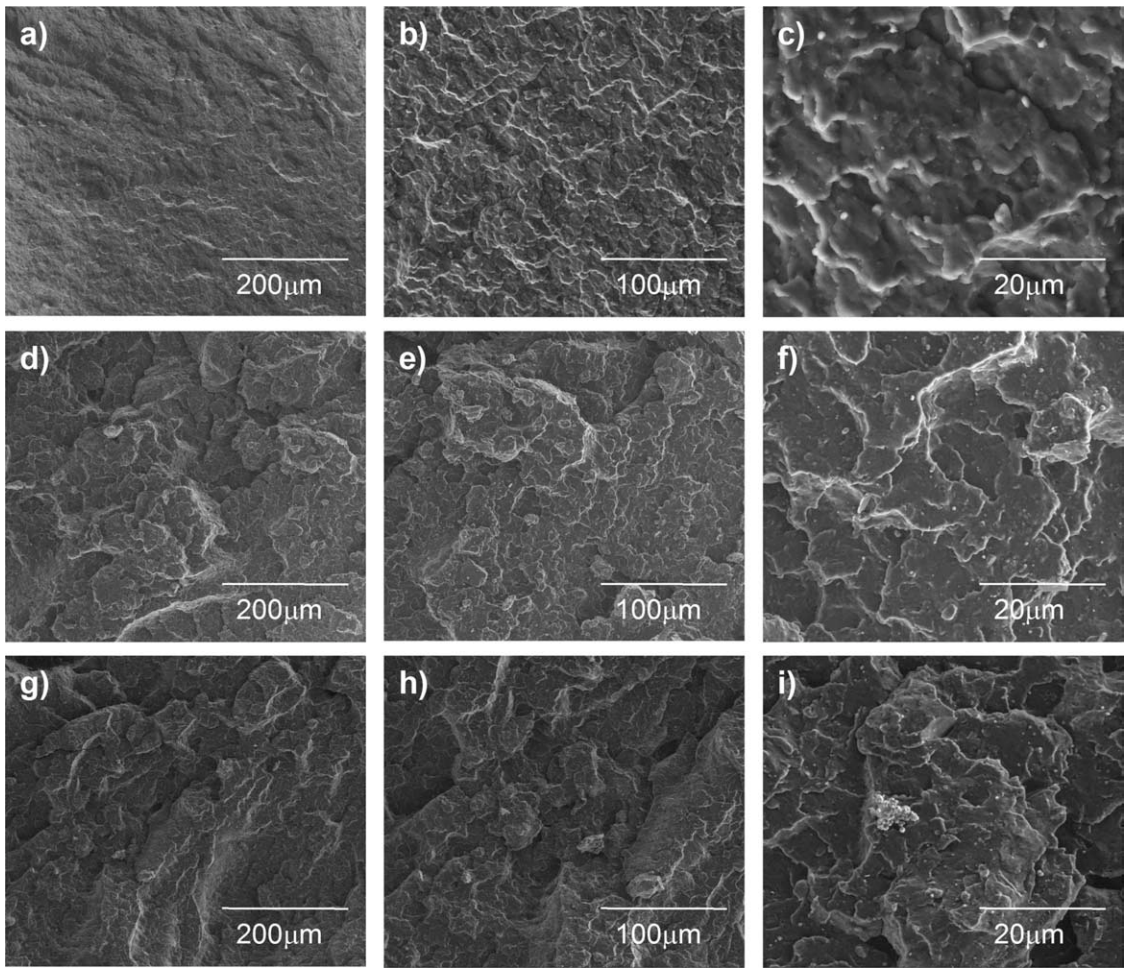

Figure 3 SEM microphotographs of fractured surfaces of POM (a–c), POM/0,5% HAp (d–f), and POM/5% HAp (g–i).

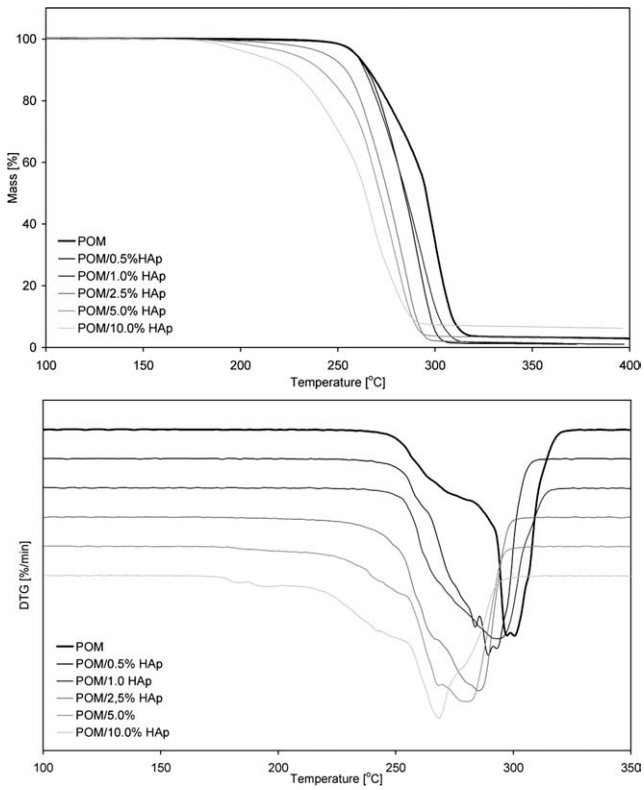

Figure 4 TG and DTG curves of pure POM and POM/HAp nanocomposites.

hypothesis that the crack path is inside the spherulites, and that cavitation occurs in the amorphous regions of the spherulite. As in rubber toughened polymers, yielding at room temperature in bulk POM is accompanied by extensive cavitation and stress whitening. Such cavitation processes enable attainment of high elongations at break without necking in tensile tests. Voiding in POM involves entanglement loss due to chain cutting. This may lead to a decrease in the density of tie molecules that interconnect the crystalline regions and, consequently, to a decrease of the load carrying capacity of the material.[37] The most smooth surface with the smallest voids of fractured sample was revealed for pure POM. It can be associated with lack of nucleating agents in the sample—it leads to homogeneous nucleation, formation of smaller amount of primary nuclei, and formation of larger and more perfect spherulitic structures. In spite of higher degree of crystallinity for POM/0.5% HAp sample, the larger amounts of voids were observed in this nanocomposite than for pure POM. In POM/HAp nanocomposites with low HAp concentraction, HAp can act as nucleating agent for POM and during POM crystallization it can be observed for both homogeneous and heterogeneous nucleation as well as more rapid POM crystallization—it leads to formation of larger amounts of spherulites which are, however, less perfect. During fracture of such a structure larger amount of voids is produced.

Thermal properties

Polyoxymethylene homopolymer is inherently unstable polymer because it degrades by depolymerization starting at the chain end on thermal unstable hydroxyl groups. Since the ceiling temperature is lower than the decomposition temperature, depolymerization is the main damage mechanism during thermal or thermomechanical loading of this polymer. Since the main chain of POM is composed of $-CH_2-O-$ bonds, the methyl oxide bonds are easy to break under heat and oxygen; they are also sensitive toward bases and acids, and this breakage results in a continuous depolymerization reaction. The formaldehyde (FA) and formic acid from the oxidized formaldehyde can accelerate such a reaction, according to "zipper" mechanism.[38] Thermal stability features POM and POM/HAp nanocomposites, prepared in the course of this work, are shown in Figure 4 and Table I.

Analysis of TG results indicates significantly lower thermal stability of POM/HAp nanocomposites in comparison to pure POM. Thermal stability of POM/HAp nanocomposites depends on content of HAp—with increase of HAp content thermal stability decreases. It should be noted that thermal stability only slightly decreases for POM/0.5% HAp and

TABLE I
TG Results for POM and POM/HAp Nanocomposites

Sample	$T_{1\%}$ (°C)	$T_{3\%}$ (°C)	$T_{5\%}$ (°C)	$T_{10\%}$ (°C)	$T_{20\%}$ (°C)	$T_{50\%}$ (°C)	T_{DTGmax} (°C)	Char residue at 400°C (%)
POM	240.5	254.8	259.1	265.6	275.3	295.4	300.4	2.64
POM/0.5% HAp	243.2	255.3	259.0	264.7	271.8	284.3	283.8 289.4	0.67
POM/1.0% HAp	241.2	256.0	259.3	263.9	270.2	285.0	293.1	1.0
POM/2.5% HAp	204.6	233.7	243.8	253.9	261.9	275.8	285.6	2.4
POM/5.0% HAp	190.4	212.8	226.4	241.0	254.6	271.8	268.3 280.3	4.3
POM/10.0% HAp	181.2	194.8	205.9	225.4	240.4	264.2	268.4	6.5

TABLE II
Temperature and Heat of Melting and Crystallization of POM and POM/HAp Nanocomposites Measured During First Heating, Cooling and Second Heating Cycles

Sample	T_{onset} (°C)	T_{max} (°C)	T_{end} (°C)	Heat of phase transition (J g^{-1})
Melting 1st run				
POM	141,08	178,2 182,3	187,14	165,29
POM/0.5% HAp	164,02	177,1 184,0	189,08	166,73
POM/1.0% HAp	168,73	177,6 182,7	187,98	167,93
POM/2.5% HAp	163,24	178,2 183,4	188,65	150,47
POM/5.0% HAp	177,98	178,9 183,3	187,85	127,66
POM/10.0% HAp	Degradation during measurement			
Crystallization				
POM	153,93	148,53	138,17	173,69
POM/0.5% HAp	154,17	149,70	139,23	180,29
POM/1.0% HAp	154,17	148,56	139,09	180,98
POM/2.5% HAp	153,86	151,02	138,04	193,87
POM/5.0% HAp	154,99	153,35	147,32	181,63
POM/10.0% HAp	Degradation			
Melting 2nd run				
POM	169,08	181,47	189,55	184,35
POM/0.5% HAp	169,53	181,63	190,37	188,71
POM/1.0% HAp	169,27	182,16	190,90	190,22
POM/2.5% HAp	170,47	177,91	189,01	164,04
POM/5.0% HAp	172,27	177,05	182,51	148,64
POM/10.0% HAp	Degradation			

POM/1.0% HAp while for higher HAp concentration the thermal stability decreases violently. The reason of lower thermal stability of POM homopolymer in POM/HAp nanocomposites is high sensitivity of main chain in POM homopolymer on base attack under heating. Hydroxyapatite with general formula $[Ca_{10}(PO_4)_6(OH)_2]$ can be also presented as $3Ca_3(PO_4)_2{\cdot}Ca(OH)_2$—a structure that contains calcium hydroxide. Moreover, nanosized HAp particles with large surface area are more reactive at elevated temperature than micrometer-size HAp. Results of DSC investigations of POM and POM/HAp nanocomposites are presented in Table II and Figure 5.

DSC results from the first heating run are strongly influenced by processing conditions (rapid cooling during injection moulding) that affect the structure and thermal properties of POM and its nanocomposites with HAp. For the first heating run during melting two maxima have been observed: the first one at $\sim 178°C$, and the second one at $\sim 183°C$. Similar effect in POM homopolymer was also observed by Bershtein et al.[39] at lower heating rates. They observed double melting peak under different heating rates, and the height and temperature of the new, second peak increased with decreasing a heating rate. This effect was attributed to reorganization or/and recrystallization processes occurring in POM crystallites, which under certain conditions are

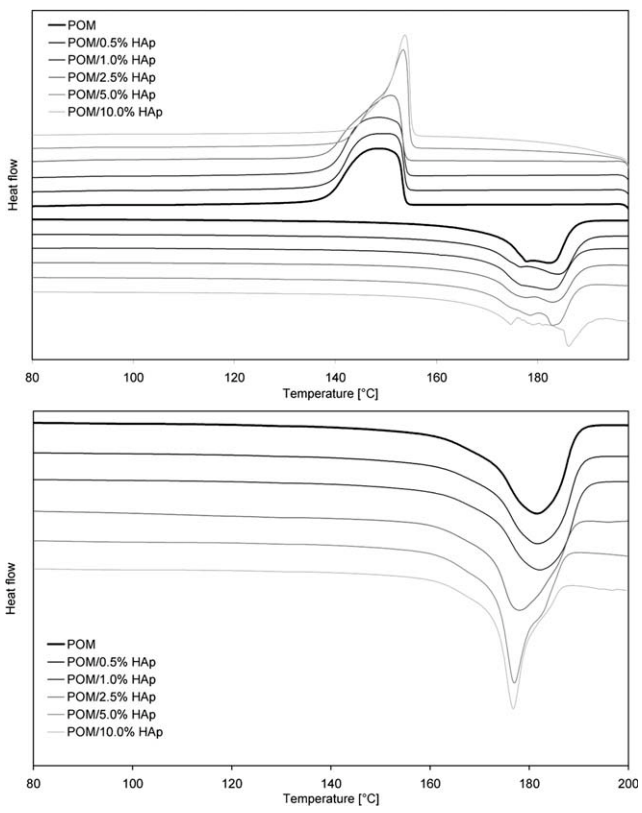

Figure 5 DSC profiles of POM/HAp nanocomposites: (a) first heating run and cooling, (b) second heating run.

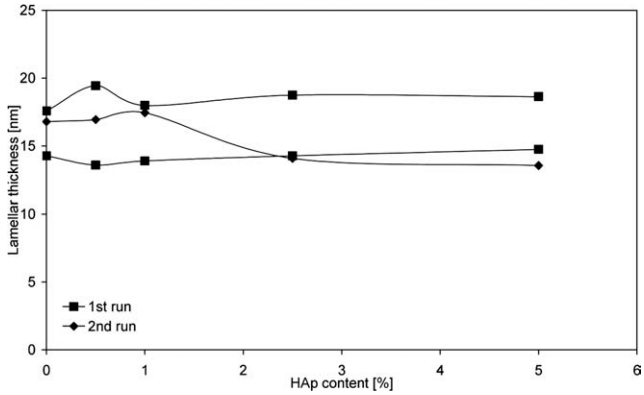

Figure 6 The variation of lamellar thickness for POM and POM/HAp nanocomposites.

metastable, as it was noted earlier.[22] On the other hand, Badrinarayanan et al.[40] investigated by rapid scanning rate DSC the effect of isothermal annealing times for poly(lactic acid) quenched from the melt (melt crystallization) and heated from the glassy state (cold crystallization) on the crystallization behavior. They observed that for both melt and cold crystallization, multiple melting behaviors at a heating rate of 500°C min^{-1} (in spite of any evidence of recrystallization during heating) occurred and suggested that the melt recrystallization theory does not offer a complete explanation of the phenomenon.

In view of these observations, double melting peak for POM could origin from its complex morphology, too. It includes extended chain crystal (ECC) and folded chain crystal (FCC) structures with different lamellar thickness (as it was described in Structure and Morphology section).

At the next stage, the lamellar thickness l of the samples was calculated using Gibbs-Thomson equation[41,42]:

$$T_{\mathrm{m}} = T_{\mathrm{m}}^{o}\left(1 - \frac{2\sigma_e}{\Delta h_o l}\right)$$

where T_m^0 is the equilibrium melting temperature, Δh_0 is thermodynamic enthalpy of fusion per unit volume of the crystalline phase, and σ_e is the free surface energy of the end faces lamellar that is associated with the crystallization process. The values of T_m^0, Δh_0, and σ_e for POM assumed in the above equation for calculating the lamellar thickness were 200°C,[43] 380 × 10^6 J m^{-3},[44] and 0.125 J m^{-2},[45] respectively.

The calculated lamellar thickness for POM and its nanocomposites during first and second heating run are shown in Figure 6.

For the first heating run, the largest difference in calculated lamellar thickness for the first and second melting maximum has been observed for POM/0.5% HAp sample—13.6 and 19.5 nm, respectively, while for pure POM l was 14.3 and 17.6 nm, respectively. For higher HAp concentration, an increase of HAp content in POM nanocomposites caused an increase of lamellar thickness for the first maximum and a decrease of lamellar thickness for the second maximum. For the second heating run (with only one maximum on DSC curves) lamellar thickness increased with an increase of HAp content up to 1.0%, and then decreased. This effect can be attributed to the formation of metastable crystallites during rapid cooling in injection mould. They show different lammellar thickness and undergo recrystallization during melting. After cooling at lower rate (10 K min^{-1}) more uniform crystals with similar melting temperatures are formed as it can be observed for the second heating run.

The degree of crystallinity (X_c) was calculated using the formula

$$X_c = \frac{\Delta H - \Delta H_a}{\Delta H_m^0} = \frac{\Delta H_m}{\Delta H_m^o}$$

where ΔH_m^0—heat of melting of 100% crystalline polymer (326.3 J g^{-1} for POM),[46] ΔH_m—heat of melting of polymer under investigation determined by DSC. X_c values of investigated samples after first and second heating run are presented in Table III.

Both for first and second heating run it can be observed that the degree of crystallinity increases with an increase of HAp content up to 1.0% and next decreases with an increase of HAp content. HAp nanoparticles up to 1.0% content act as effective nucleating sites, whereby for higher HAp concentrations the nanofiller act as impurity and hinder POM crystallization. It also should be noted that higher degree of crystallinity was observed for the second heating run—it confirms previous

TABLE III
Heat of Melting and Degree of Crystallinity of Pristine POM and POM in POM/HAp Nanocomposites

Sample	POM heat of melting (J g^{-1})	Degree of crystallinity (%)
Melting 1st run		
POM	165.29	50.66
POM/0.5% HAp	167.57	51.35
POM/1.0% HAp	169.63	51.98
POM/2.5% HAp	154.33	47.30
POM/5.0% HAp	134.38	41.18
POM/10.0% HAp	Degradation	–
Melting 2nd run		
POM	184.35	56.50
POM/0.5% HAp	189.66	58.12
POM/1.0% HAp	192.14	58.88
POM/2.5% HAp	168.25	51.56
POM/5.0% HAp	156.46	47.95
POM/10.0% HAp	Degradation	–

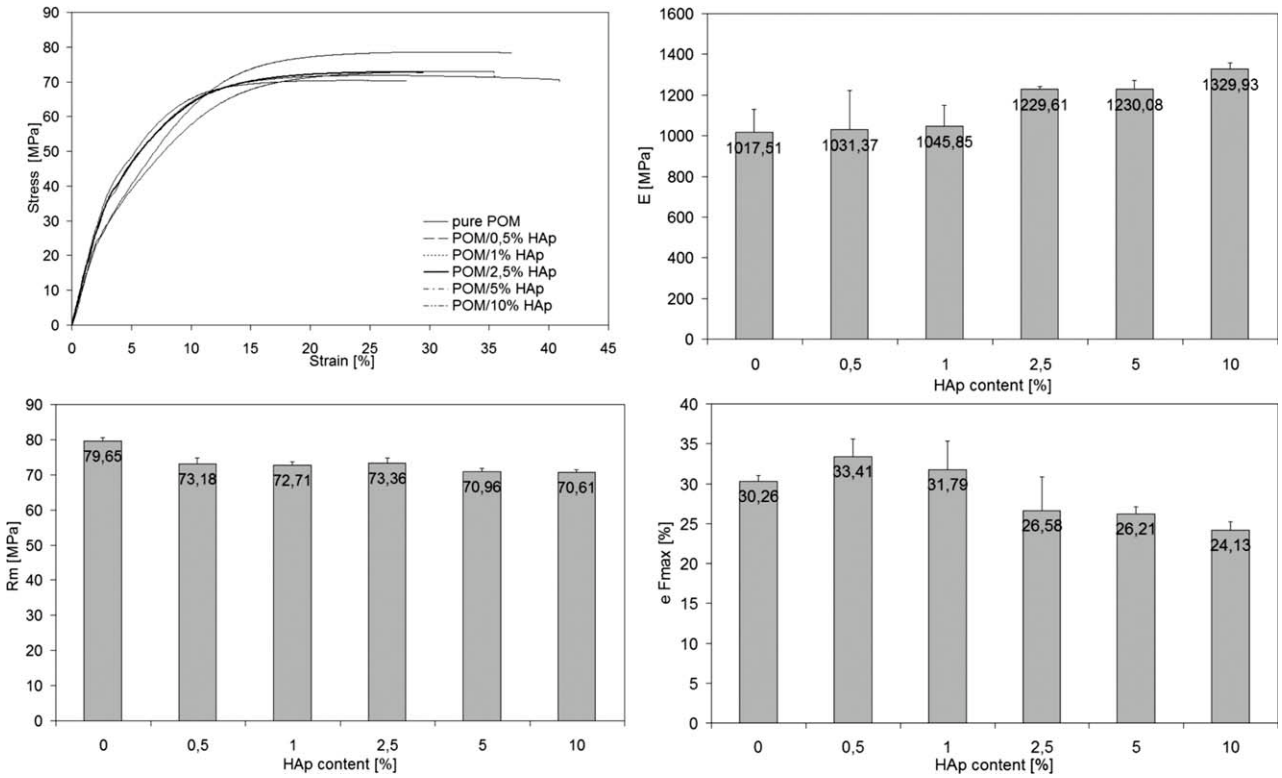

Figure 7 Tensile properties of POM and POM/HAp nanocomposites.

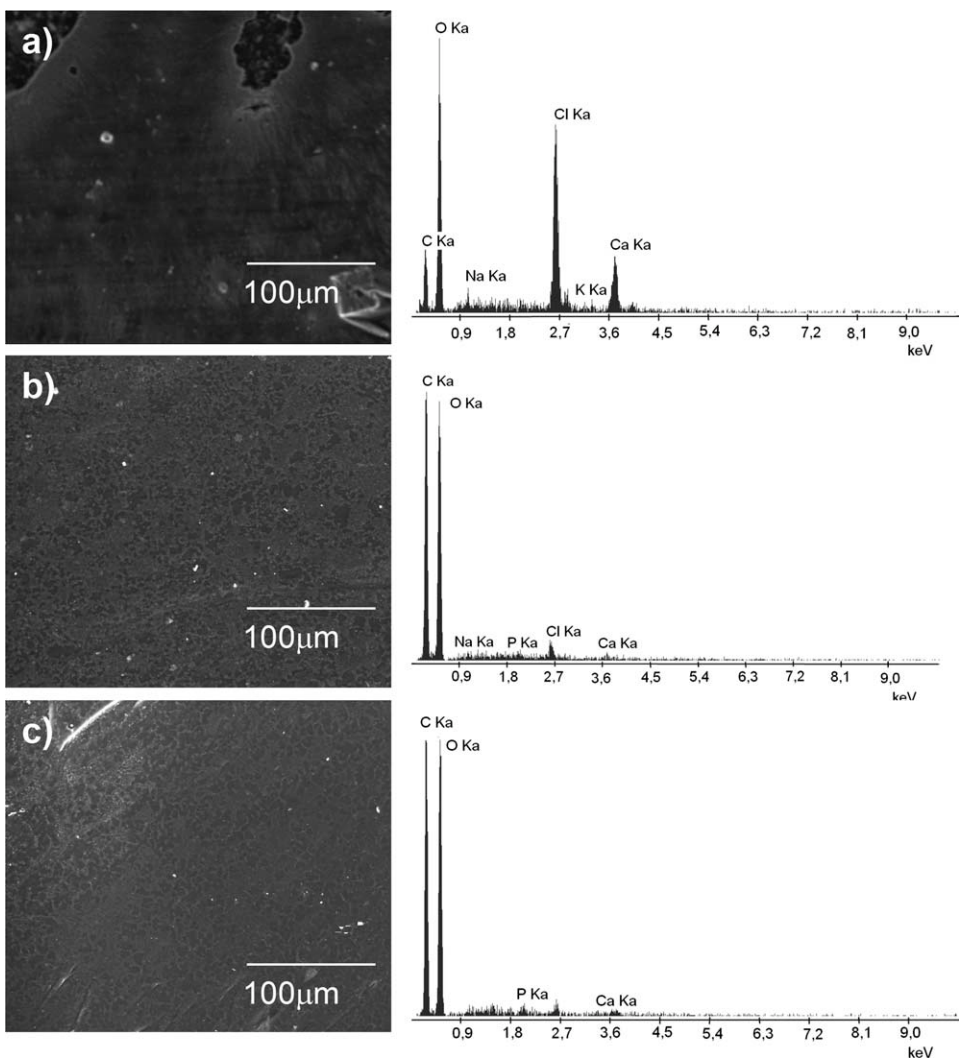

Figure 8 SEM microphotographs and EDX analysis after 7 days of incubation in SBF: POM (a), POM/0.5% HAp (b), POM/5.0% Hap (c).

observation that in injection moulding conditions a fraction of metastable crystallites as well as large amount of amorphous phase are formed.

Tensile properties

A typical group of stress-strain curves and the changes in mechanical properties of POM and POM/HAp nanocomposites as a function of hydroxyapatite concentration are shown in Figure 7.

It can be seen that, Young's modulus increases with increasing hydroxyapatite concentration, elongation at break decreases with increasing HAp concentration and tensile strength decreases slightly with HAp concentration. The change in mechanical properties is the result of the changes in crystal size owing to the existence of the nucleating agent HAp and changes in samples morphology. It should be noted that between samples with the highest degree of crystallinity (POM, POM/0.5% HAp and POM/1.0% HAp) and with lowest crystallinity (POM/2.5% HAp, POM/5.0% HAp and POM/10.0% HAp) significant jump in mechanical properties has been observed. Samples with highest degree of crystallinity have lower Young's modulus and higher elongation at break. Moreover, during tensile tests whitening and elongations at break without necking for all samples was observed.

In vitro evaluation

In vitro evaluation is a fundamental procedure to assess the bioactivity and biostability of tested synthetic material. POM, POM/0.5% HAp and POM/5.0% HAp have been immersed in SBF for 7 days, and then the sufrace morphology analyzed by SEM-EDX – Figure 8.

Figure 8(a) shows the surface morphology of pure POM and results of average EDX analysis of the sample surface after 7 days immersion in SBF—the results of EDX analysis show that pure POM in an inert material in SBF and it does not induce HAp formation, but induce formation chlorides, which is an unfavourable effect. Figure 8(b,c) show the surface morphology and results of average EDX analysis of POM/0.5% HAp and POM/5.0% HAp after 7-day immersion. The obtained results confirmed bioactivity of POM/5.0% HAp sample—it can be seen formation of apatite layer on the surface, while for POM/0.5% HAp formation both apatie and chloride layer. The largest intensity of peaks from apatites in EDX results was observed for POM/5.0% HAp—with an increase of HAp content in nanocomposites, their bioactivity and formation of apatite layer increase and, formation of chlorides on the sample surface decreases.

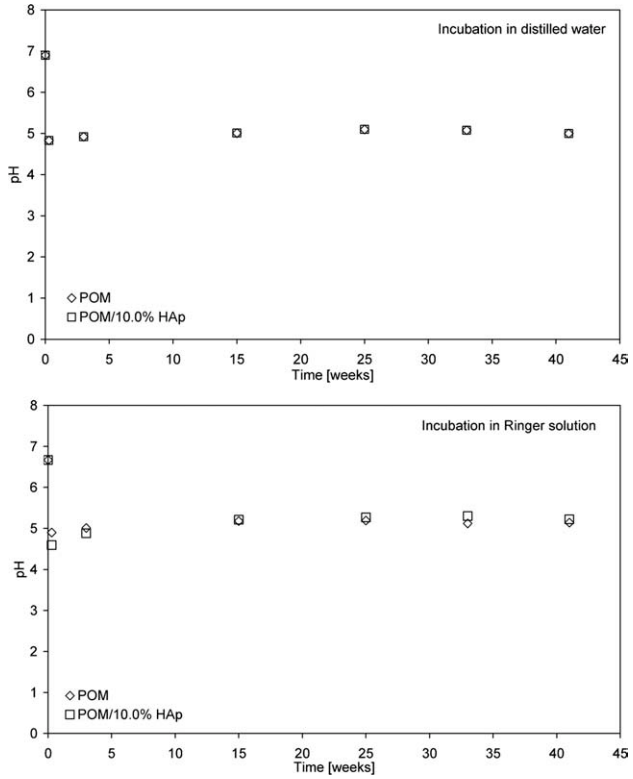

Figure 9 pH changes of distilled water and Ringer solution as a function of incubation time of POM and POM/10.0% HAp samples.

In vitro stability of POM and POM/10.0% HAp samples was determined on the basis of pH variations of distilled water and Ringer solution, and mass changes of the samples during POM and POM nanocomposite incubation at the temperature 70°C during 41 weeks (according to EN ISO 10933—an accelerated degradation test as a screening method). Time of incubation was elongated to 9 months (usually for accelerated method time of incubation is 60 days) for confirmation good long-term stability of POM even at elevated temperature—Figure 9.

Figure 9 shows the lack of significant pH changes both of water and Ringer solution during incubation of the POM-based materials. It was also observed no significant difference in *in vitro* behavior between pure POM and POM/10.0% HAp nanocomposite. Moreover, mass of the samples did not change after incubation. The obtained results confirmed very good *in vitro* stability of POM and POM/HAp nanocomposites.

CONCLUSIONS

Novel POM/HAp nanocomposites for bone long-term implants have been obtained by melt processing technique. The highest melting temperature and degree of crystallinity were found by DSC method for POM/0.5% HAp. In these composites HAp

nanoparticles act as effective nucleating sites. Moreover, no shift in 2θ for pure POM and POM with hydroxyapatite was observed, indicating that the addition of HAp does not change the hexagonal system of POM. Young's modulus was found to increase with HAp concentration, whereby longation at break and tensile strength decrease with higher HAp content. The *in vitro* evaluation shows that addition of HAp to POM matrix improve bioactivity of the nanocomposites and after 41 weeks of incubation no changes in nanocomposites' mass have been observed, confirming very good *in vitro* stability of POM/HAp nanomaterials.

References

1. Bhowmik, R.; Kalpana, C.; Katti, S.; Dinesh, C.; Katti, R. J Mater Sci 2007, 42, 8795.
2. Kenny, S. M.; Buggy, M. J Mater Sci Mater Med 2003, 14, 923.
3. Middleton, J. C.; Tipton, A. J. Biomaterials 2000, 21, 2335.
4. Liu, X.; Ma, P. X. Biomed Eng 2004, 32, 477.
5. Bouyer, E.; Gitzhofer, F.; Boulos, M. I. J Mater Sci Mater Med 2000, 11, 523.
6. Pielichowska, K.; Blazewicz, S. Adv Polym Sci 2010, 232, 97.
7. Luftl, S.; Archodoulaki, V. M.; Seidler, S. Polym Degrad Stab 2006, 91, 464.
8. Masamoto, J. Prog Polym Sci 1993, 18, 1.
9. Pielichowski, K.; Flejtuch, K. Polimery 2004, 49, 80.
10. Sanchez-Soto, M.; Illescas, S.; Milliman, H.; Schiraldi, D. A.; Arostegui, A. Macromol Mater Eng 2010, 295, 846.
11. Masirek, R.; Piórkowska, E. Eur Polym J 2010, 46, 1436.
12. Siengchin, S.; Psarras, G. C.; Karger-Kocsis, J. J Appl Polym Sci 2010, 117, 1804.
13. Zhao, X. W.; Ye, L. J Polym Sci Part B Polym Phys 2010, 48, 905.
14. Thompson, M. S.; Northmore-Ball, M. D.; Tanner, K. E. J Mater Sci Mater Med 2001, 12, 883.
15. Thompson, M. S. Design of a Novel Hip Resurfacing Prosthesis, Ph. D Thesis; London, 2001.
16. Moore, D. J.; Freeman, M. A.; Revell, P. A.; Bradley, G. W.; Tuke, M. J Arthroplasty 1998, 13, 388.
17. McKellop, H. A.; Milligan, H. L.; Röstlund, T. J Heart Valve Dis 1996, 5, 238.
18. Zilberman, U. Am J Orthodont Dentofac Orthop 2005, 128, 147.
19. Kokubo, T.; Takadama, H. Biomaterials 2006, 27, 2907.
20. Carazzolo, G. A. J Polym Sci A Gen Pap 1963, 1, 1573.
21. Tadokoro, H.; Yasumoto, T.; Murashashi, S.; Nitta, J. J Polym Sci 1960, 44, 266.
22. Jaffe, M.; Wunderlich, B.KolloidZ. U. Z. Polymere 1967, 216/217, 203.
23. Schweizer, T.; Vancso, G. Angew Makromol Chem 1989, 173, 85.
24. Xu, W. B.; He, P. S. Polym Eng Sci 2001, 41, 1903.
25. Maeda, Y.; Nakayama, K.; Kanetsuna, H. Polym J 1982, 14, 649.
26. Taraiya, A. K.; Unwin, A. P.; Ward, I. M. J Polym Sci B Polym Phys 1988, 26, 817.
27. Reneker, D. H.; Geil, P. H. J Appl Phys 1960, 31, 1916.
28. Bassett, D. C. Phil Mag 1964, 10, 595.
29. Garber, C. A.; Geil, P. H. Makromol Chem 1968, 113, 236.
30. Iguchi, M. Br Polym J 1973, 5, 195.
31. Iguchi, M.; Murase, I. J Polym Sci Polym Phys 1975, 13, 1461.
32. Shimomura, M.; Iguchi, M. Polymer 1982, 23, 509.
33. Shimomura, M.; Iguchi, M.; Kobayashi, M. Polymer 1988, 29, 351.
34. Kobayashi, M.; Sakashita, M. J Chem Phys 1992, 96, 748.
35. Hama, H.; Tashiro, K. Polymer 2003, 44, 3107.
36. Hama, H.; Tashiro, K. Polymer 2003, 44, 2159.
37. Lazzeri, A.; Marchetti, A.; Levita, G. Fatigue Fract Eng Mater Struct 1997, 20, 1207.
38. Shi, J.; Jing, B.; Zou, X.; Luo, H.; Dai, W. J Mater Sci 2009, 44, 1251.
39. Bershtein, V. A.; Egorova, L. M.; Egorov, V. M.; Peschanskaya, N. N.; Yakushev, P. N.; Keating, M. Y.; Flexman, E. A.; Kassal, R. J.; Schodt, K. P. Thermochim Acta 2002, 391, 227.
40. Badrinarayanan, P.; Dowdy, K. B.; Kessler, M. R. Polymer 2010, 51, 4611.
41. Mohanraj, J.; Bonner, M. J.; Barton, D. C.; Ward, I. M. Polymer 2006, 47, 5897.
42. Wunderlich, B. Macromolecular Physics; Academic: New York, 1980.
43. Salaris, F.; Turturro, A.; Bianchi, U.; Martuscelli, E. Polymer 1978, 19, 1163.
44. Brandrup, J.; Immergut, E. H. Polymer Handbook, 3rd ed.; Wiley: New York, 1989.
45. Plummer, C. J. G.; Menu, P.; Cudremauroux, N.; Kausch, H. H. J Appl Polym Sci 1995, 55, 489.
46. Available at: http://athas.prz.rzeszow.pl/.